JOURNAL OF COMPUTATIONAL PHYSICS 122, 307–316 (1995)

Non-Reflecting Boundary Conditions for the Steady Euler Equations

LARS FERM

Department of Scientific Computing, Uppsala University, Uppsala, Sweden

Received November 16, 1992; revised April 25, 1995

Artificial boundary conditions for the steady Euler equations in a channel are considered. Non-reflecting terms are added to the boundary conditions to accelerate the convergence to the steady state. The aim of the article is to investigate how the steady and non-reflecting parts of the combined conditions should be balanced. It turns out that the scaling of the non-reflecting terms depends on the solution and on the size of the computational region. Numerical examples are presented. © 1995 Academic Press, Inc.

1. INTRODUCTION

Artificial boundaries are often needed in computational problems to make unbounded regions bounded. A problem is that data usually are missing at these boundaries. We thus need boundary conditions which lead to good solutions even if data are missing.

For time dependent problems artificial boundary conditions should annihilate waves coming from the interior. Otherwise waves are reflected back into the domain at the non-physical boundary. Such non-reflecting conditions have been developed for a large number of problems. An overview is given by Givoli [9]. Some examples are [12, 3, 10, 11].

Many non-reflecting conditions lead to steady solutions of poor accuracy. The steady solution may depend on the initial one which we do not know how to choose. On the other hand, non-reflecting conditions often lead to rapid convergence to the steady state. We are thus interested in non-reflecting conditions which lead to accurate steady solutions. Bayliss and Turkel [1] derive non-reflecting conditions for the Euler equations which they use for steady state calculations. The boundary conditions are obtained from expansions of the solution at large distances.

Very accurate boundary conditions for the steady Euler equations in a channel are studied in [5, 7, 8]. The corresponding conditions for the external problem also lead to accurate solutions but they are more complicated to use [6].

The steady problem can be solved with a direct solver or with a time-marching procedure in the interior. Newton's method is used in [7, 5] to solve the discretized steady Euler equations in a channel directly. The converged solutions are obtained within three or four iterations using different boundary conditions including the exact steady ones.

When time-marching methods are used in the interior the situation is very different. The steady conditions for the Euler equations often lead to large numbers of time steps before the steady states are reached. The solution might even not converge. It is thus necessary to improve the convergence to the steady state.

Waves coming perpendicular to the boundary from the interior are not reflected back if the characteristic variables corresponding to ingoing characteristics are kept fixed in time [3, 4, 10]. Therefore Engquist and Halpern [2] differentiate these characteristic variables with respect to time and add them to the steady conditions. Thus these characteristic variables vary more slowly in time at the boundary, but we still expect the same steady solution as with the unmodified steady conditions. This combined technique is used for the Euler equations in a periodic channel by Giles [8]. Rudy and Strikwerda [14, 15] use the same idea for another steady condition. A problem is how to scale the non-reflecting terms in the combined conditions. This problem is solved in [14] for the case when the steady conditions specify the outflow pressure and the inflow velocity. The combined technique is used at the outflow boundary. The analysis is one-dimensional.

The aim of this article is to study the scaling of non-reflecting terms added to the accurate steady conditions for the Euler equations in a channel. The steady and combined boundary conditions are described in Section 2. The mean values of the solution across the boundary are treated separately by the steady conditions. The treatment of the mean values is considered in Section 3. The scaling parameters of the combined conditions are studied in Section 4. The method by Rudy and Strikwerda [14] is used to optimize the parameters. We show that the scaling depends on the speed of sound and the length of the channel. Numerical examples are presented in Section 5. Some conclusions are given in Section 6.

2. THE BOUNDARY CONDITIONS

We consider flow in an infinitely long channel with straight walls outside a bounded region. Introduce an artificial inflow boundary $x = a$ to the left of the bounded region and an artificial outflow boundary $x = b$ to the right. Two examples are given in Fig. 2. The artificial boundaries are the dashed lines $x =$

0021-9991/95 $12.00

$a = 0$ and $x = b = 1$. The boundary conditions are intended for problems where the flow is subsonic on and outside the artificial boundaries. The boundary should thus be moved outside supersonic areas of the solution.

The boundary conditions are designed to be satisfied exactly in the region outside the artificial boundary by the solution of the linearized steady Euler equations

$$A\mathbf{w}_x + B\mathbf{w}_y = 0, \tag{1}$$

where

$$A = \begin{pmatrix} \bar{u} & \bar{\rho} & 0 & 0 \\ 0 & \bar{u} & 0 & 1/\bar{\rho} \\ 0 & 0 & \bar{u} & 0 \\ 0 & \bar{c}^2\bar{\rho} & 0 & \bar{u} \end{pmatrix}, \quad B = \begin{pmatrix} 0 & 0 & \bar{\rho} & 0 \\ 0 & 0 & 0 & 0 \\ 0 & 0 & 0 & 1/\bar{\rho} \\ 0 & 0 & \bar{c}^2\bar{\rho} & 0 \end{pmatrix}, \tag{2}$$

$$\mathbf{w} = \begin{pmatrix} \rho \\ u \\ v \\ p \end{pmatrix}.$$

Note that we may linearize around different states for the inflow and outflow boundary conditions.

2.1. *The Steady Boundary Conditions*

Introduce the Fourier expansions

$$\begin{pmatrix} p(x,y) \\ u(x,y) \\ \rho(x,y) \end{pmatrix} = \sum_{\omega=0}^{\infty} \begin{pmatrix} \hat{p}_\omega(x) \\ \hat{u}_\omega(x) \\ \hat{\rho}_\omega(x) \end{pmatrix} \cos\frac{\pi\omega y}{L_y}, \tag{3}$$

$$v(x,y) = \sum_{\omega=1}^{\infty} \hat{v}_\omega(x) \sin\frac{\pi\omega y}{L_y}, \tag{4}$$

where L_y is the width of the channel on and outside the boundary, and the lower channel wall is $y = 0$. The inflow boundary conditions for $\omega > 0$ are

$$\hat{v}_\omega(a) = \eta_a \hat{p}_\omega(a), \tag{5}$$

$$(\hat{p}_\omega - \bar{c}^2\hat{\rho}_\omega)(a) = 0, \tag{6}$$

$$(\hat{p}_\omega + \bar{\rho}\bar{u}\hat{u}_\omega)(a) = 0, \tag{7}$$

and the outflow condition is

$$\hat{p}_\omega(b) = -\frac{1}{\eta_b}\hat{v}_\omega(b). \tag{8}$$

Here η_a and η_b are the inflow and outflow values of

$$\eta = \frac{\sqrt{1-M^2}}{\bar{c}\bar{\rho}M},$$

where M is the Mach number $M = \bar{u}/\bar{c}$. Conditions (6) and (7) can be written as

$$(\tilde{p} - \bar{c}^2\tilde{\rho})(a,y) = 0, \tag{9}$$

$$(\tilde{p} + \bar{\rho}\bar{u}\tilde{u})(a,y) = 0, \tag{10}$$

where $\tilde{p}$, $\tilde{u}$, $\tilde{\rho}$ are defined by

$$\tilde{p}(x,y) = p(x,y) - \hat{p}_0(x), \tag{11}$$

$$\tilde{u}(x,y) = u(x,y) - \hat{u}_0(x), \tag{12}$$

$$\tilde{\rho}(x,y) = \rho(x,y) - \hat{\rho}_0(x). \tag{13}$$

This saves Fourier transformations at the inflow boundary. We have only given conditions for $\omega > 0$. The conditions of $\omega = 0$ are found in Section 3.

2.2. *The Combined Conditions*

The combined technique is intended to speed up the convergence to the steady state without destroying the accuracy of the converged solution. The Fourier transformed linearized time-dependent Euler equations are

$$\hat{w}_t + A\hat{w}_x + \omega\pi\hat{B}\hat{w} = 0, \tag{14}$$

where

$$\hat{B} = \begin{pmatrix} 0 & 0 & \bar{\rho} & 0 \\ 0 & 0 & 0 & 0 \\ 0 & 0 & 0 & -1/\bar{\rho} \\ 0 & 0 & \bar{c}^2\bar{\rho} & 0 \end{pmatrix}.$$

The Fourier transformed characteristic variables are

$$\hat{\Psi} = \begin{pmatrix} \hat{\Psi}_1 \\ \hat{\Psi}_2 \\ \hat{\Psi}_3 \\ \hat{\Psi}_4 \end{pmatrix} = T\hat{w} = \begin{pmatrix} \bar{c}^2 & 0 & 0 & -1 \\ 0 & \bar{c}\bar{\rho} & 0 & 1 \\ 0 & 0 & 1 & 0 \\ 0 & \bar{c}\bar{\rho} & 0 & -1 \end{pmatrix} \begin{pmatrix} \hat{\rho} \\ \hat{u} \\ \hat{v} \\ \hat{p} \end{pmatrix}. \tag{15}$$

According to the directions of the characteristics, we set at the inflow boundary

$$\hat{\Psi}_{in} = \begin{pmatrix} \hat{\Psi}_1 \\ \hat{\Psi}_2 \\ \hat{\Psi}_3 \end{pmatrix}, \quad \hat{\Psi}_{out} = \hat{\Psi}_4,$$

and vice versa at the outflow boundary. For $\omega = 0$ we omit $\hat{\Psi}_3$ in these vectors since v is expanded in a sine series. At each boundary the steady conditions can be written

$$\hat{\Psi}_{in} = S\hat{\Psi}_{out}, \tag{16}$$

while

$$\frac{\partial}{\partial t}\hat{\Psi}_{in} = 0, \tag{17}$$

is a non-reflecting condition. A natural way to combine the conditions is

$$\left(\alpha\frac{\partial}{\partial t} + I\right)\hat{\Psi}_{in} = S\hat{\Psi}_{out}, \tag{18}$$

where $\alpha = \text{diag}(\alpha_i)$. The parameters α_i are chosen by the user.

The non-reflecting terms can be applied when the solution has been transformed back to the physical space after the application of the steady conditions. Otherwise extra Fourier transformations are needed at the inflow boundary. It also turns out that we often get a slightly better convergence in the end of the process approaching the accuracy of the computer. The methods are otherwise equivalent. The non-reflecting step is thus applied as

$$\left(\alpha\frac{\partial}{\partial t} + I\right)\Psi_{in} = \Psi^S_{in}, \tag{19}$$

where the vector Ψ_{in} contains characteristic variables of the physical problem at all discrete boundary points. The vector Ψ^S_{in} contains the values obtained when the unmodified steady conditions are applied.

The mean values of the solution are treated separately by the steady conditions. Hence we expect that they should be treated separately in the non-reflecting step as well. This is discussed in Section 3.

3. THE MEAN VALUES

Since we only consider the case $\omega = 0$, $\hat{\Psi}_i$ in this section always denotes the mean value of the characteristic variable Ψ_i.

3.1. *The Steady Mean Value Conditions*

Consider the Fourier transformed Euler equations (14). The steady solution is independent of x for $\omega = 0$. Free-stream data can thus be used for the mean values at the boundaries. The amount of available data on each side determines which mean-value conditions can be used. If possible we choose conditions which lead to rapid convergence to the steady state. If a time-marching procedure is used for the calculations in the interior, we consider the number of characteristics entering the doman at each boundary. We are not interested in the mean value of v since v is expanded in a sine series. Two characteristics not involving v enter the domain at the inflow boundary and one at the outflow boundary. Hence, two mean value conditions are needed at the inflow boundary, and one mean value condition is needed at the outflow boundary. If enough free-stream data are available, we can use characteristic boundary conditions for the mean values. We assume that we can use characteristic conditions at the inflow boundary, i.e.,

$$\hat{\Psi}_1(a) = p_{-\infty} - \bar{c}^2\rho_{-\infty}, \tag{20}$$

$$\hat{\Psi}_2(a) = \overline{c\rho}u_{-\infty} + p_{-\infty} = g_2. \tag{21}$$

The outflow mean value condition can be chosen from, for example,

$$\hat{\Psi}_4(b) = \overline{c\rho}u_\infty - p_\infty, \tag{22}$$

$$\hat{p}_0(b) = p_\infty, \tag{23}$$

$$\int_{y1}^{y2} \rho(b, y)u(b, y)\,dy = u_{-\infty}\rho_{-\infty}L_{in}, \tag{24}$$

where y_1, y_2 define the channel walls to the right and L_{in} is the width of the channel to the left. The amount of needed downstream data differs between these conditions. Condition (24) requires no downstream data at all. It reflects the fact that the mass flow per unit time across any line across the channel is equal when the steady state is reached.

3.2. *Non-reflecting Conditions for the Mean Values*

Consider the Fourier transformed system (14). It is very simple for $\omega = 0$, and it is diagonalized by the matrix T. The values of the characteristic variables follow exactly the characteristics. Assume that we use the inflow condition (21) and the outflow condition (23). The characteristic variable $\hat{\Psi}_2$ is at the steady state in the whole domain for $t \geq t_1 = (b - a)/(\bar{c} + \bar{u})$, and $\hat{\Psi}_4$ is at the steady state in the whole domain for $t \geq t_2 = t_1 + (b - a)/(\bar{c} - \bar{u})$. The combined condition corresponding to the outflow condition (23) is

$$\left(\alpha\frac{\partial}{\partial t} + I\right)\hat{\Psi}_4(b, t) = \hat{\Psi}_2(b, t) - 2p_\infty = g(t), \tag{25}$$

where

$$g(t) = \begin{cases} \hat{\Psi}_2(x - (c + u)t, 0) - 2p_\infty & \text{for } t < t_2 \\ g_4 & \text{for } t \geq t_2 \end{cases}$$

and $g_4 = g_2 - 2p_\infty$. For $\alpha > 0$ we get

$$\hat{\Psi}_4(b, t) = \hat{\Psi}_4(b, 0)e^{-t/\alpha} + \int_0^t \frac{1}{\alpha} e^{(s-t)/\alpha} g(s)\, ds, \tag{26}$$

which for $t > t_2$ gives

$$\hat{\Psi}_4(b, t) = \hat{\Psi}_4(b, t_2)e^{-(t-t_2)/\alpha} + g_4(1 - e^{-(t-t_2/\alpha)}). \tag{27}$$

As an example we consider a linear initial state $\hat{\Psi}_2(x, 0)$. It is easily verified for $\alpha > 0$ that the mean values are not at the steady state at $t = t_3$ unless $\hat{\Psi}_2(x, 0) \equiv g_2$ in the whole domain. We thus expect slower convergence due to the non-reflecting term. In practical calculations the convergence of the mean values is so rapid anyway that we can disregard this slower convergence. The exception is when the mass flow condition (24) is used at the outflow boundary. We recommend avoiding the non-reflecting mean value term for this condition.

The mean values $\hat{u}_0$, $\hat{p}_0$ are decoupled from the rest of the Fourier transformed system (14). Consider using the outflow condition (23) and the inflow condition

$$\hat{u}_0(a, t) = u_{-\infty}, \tag{28}$$

or, equivalently,

$$\hat{\Psi}_2(a, t) = -\hat{\Psi}_4(a, t) + 2\overline{\rho c} u_{-\infty}. \tag{29}$$

By following the characteristics two times back and fourth across the region, we get

$$\hat{\Psi}_4(b, t + 2t_3) = \hat{\Psi}_4(b, t).$$

Convergence is thus only obtained if the mean values are equal to the initial state all the time. The corresponding combined outflow condition (25) can be written

$$-\frac{\partial}{\partial t}\hat{\Psi}_4(b, t) + \alpha_R(\hat{p}_0(b, t) - p_\infty) = 0, \tag{30}$$

with $\alpha_R = 0.5/\alpha$. This is the mean value version of the outflow condition by Rudy and Strikwerda [14]. They use the condition for the whole solution, not only $\hat{p}_0$. This means that the converged pressure is constant along the outflow boundary and a larger region is needed for good accuracy. However, they study the equations for $\omega = 0$ and optimize the choice of α_R using the boundary conditions (30), (28). Their result is thus applicable for this set of mean value conditions. Their result is not applicable if we use the inflow condition (21), for which we have observed that the mean values reach the steady state in finite time without non-reflecting terms.

4. SCALING THE NON-REFLECTING TERMS

The combined conditions (19) contain undetermined coefficients α_i. The choice of these coefficients is studied in this section.

4.1. *Scaling the Dependent Variables*

The transformations

$$\rho^* = \rho/\overline{\rho}, \quad p^* = p/\overline{p}, \quad u^* = u/\overline{c}, \quad v^* = v/\overline{c}, \quad t^* = \overline{c}t,$$

lead to the non-dimensionalized Euler equations

$$\hat{w}_t^* + A^*\hat{w}_x^* + \hat{B}^*\hat{w}_y^* = 0, \tag{31}$$

where

$$A^* = \begin{pmatrix} M & 1 & 0 & 0 \\ 0 & M & 0 & \frac{1}{\gamma} \\ 0 & 0 & M & 0 \\ 0 & \gamma & 0 & M \end{pmatrix}, \quad \hat{B}^* = \begin{pmatrix} 0 & 0 & 1 & 0 \\ 0 & 0 & 0 & 0 \\ 0 & 0 & 0 & -\frac{1}{\gamma} \\ 0 & 0 & \gamma & 0 \end{pmatrix}, \tag{32}$$

and M is the Mach number $\overline{u}/\overline{c}$. The characteristic variables corresponding to $\hat{\Psi}$ are denoted by $\hat{\Psi}^*$. The combined conditions for the non-dimensionalized problem are

$$\beta\frac{\partial}{\partial t^*}(\hat{\Psi}_{\text{in}}^*) + \hat{\Psi}_{\text{in}}^* = S^*\hat{\Psi}_{\text{out}}^*, \tag{33}$$

where $\beta = \text{diag}\,(\beta_i)$. Here S^* denotes the steady conditions for the non-dimensionalized problem. When condition (33) is transformed to the original variables, we get

$$\alpha_i = \beta_i/\overline{c}. \tag{34}$$

4.2. *Scaling Due to the Length of the Channel*

The Euler equations

$$w_t + Aw_x + Bw_y = 0$$

take the same form after the variable transformations

$$\tilde{x} = x/L, \quad \tilde{y} = y/L, \quad \tilde{t} = t/L,$$

but the combined condition

$$\left(\alpha\frac{\partial}{\partial t} + I\right)\Psi_{\text{in}} = S\Psi_{\text{out}}$$

is transformed into

$$\left(\frac{1}{L}\alpha\frac{\partial}{\partial\tilde{t}}+I\right)\tilde{\Psi}_{\text{in}}=S\tilde{\Psi}_{\text{out}},$$

where

$$\tilde{\Psi}(\tilde{x},\tilde{y},\tilde{t})=\Psi(x,y,t).$$

The independent variables must thus be normalized for a general choice of the parameters. The only meaningful scaling for the mean values is the distance between the outflow and inflow boundaries denoted by L_x. Assume that the optimum parameters are β_i when $L_x = c = 1$. The results in Subsections 4.1 and 4.2 show that the optimum parameters for the original equations are

$$\alpha_i=\beta_i\frac{L_x}{\bar{c}}.$$

4.3. *Optimizing the Coefficients*

We use the one-dimensional analysis by Rudy and Strikwerda [14]. The relevance of the results for the two-dimensional problem will be studied experimentally. We linearize the Euler equations, delete the derivatives with respect to y, and diagonalize the system to

$$\Psi_t+\Lambda\Psi_x=0,$$

where $\Lambda = \text{diag}\,(\bar{u}, \bar{c}+\bar{u}, \bar{u}, \bar{u}-\bar{c})$. The combined conditions for the characteristic variables corresponding to the steady conditions (5), (8), (6), (7) are

$$\left(\alpha_1\frac{\partial}{\partial t}+I\right)\Psi_1=0 \tag{35}$$

$$\left(\alpha_2\frac{\partial}{\partial t}+I\right)\Psi_2=\frac{1-M}{1+M}\Psi_4 \tag{36}$$

$$\left(\alpha_3\frac{\partial}{\partial t}+I\right)\Psi_3=-\eta_a\frac{M}{1+M}\Psi_4 \tag{37}$$

at the inflow boundary. The outflow condition is

$$\left(\alpha_4\frac{\partial}{\partial t}+I\right)\Psi_4=\Psi_2+\frac{2}{\eta_b}\Psi_3. \tag{38}$$

To make the analysis possible, we consider one coefficient at a time, and set

$$\alpha_1=\alpha_3=0,\ \alpha_2=\infty$$

when optimizing α_4. The choice of α_2 means that we specify Ψ_2; i.e., $\Psi_2 = 0$. Assume that the artificial boundaries are $x = 0$ and $x = L_x$. The solutions have the form

$$\Psi_2=\gamma_2 e^{-z(t-\lambda_2 x)}, \tag{39}$$

$$\Psi_3=\gamma_3 e^{-z(t-\lambda_3 x)}, \tag{40}$$

$$\Psi_4=\gamma_4 e^{-z(t-\lambda_4 x)}, \tag{41}$$

where $(\lambda_2, \lambda_3, \lambda_4) = (1/\bar{u}+\bar{c}),\ 1/\bar{u},\ (1/\bar{u}-\bar{c})$. The inflow boundary conditions lead to $\gamma_2 = 0$, and assuming that $\eta_a = \eta_b = \eta$, we get

$$\gamma_3=-\eta\alpha\gamma_4/2,$$

where

$$a=\frac{2M}{1+M}.$$

The outflow boundary condition leads to

$$1-\alpha_4 z=-ae^{z\tau}, \tag{42}$$

where $\tau = (\lambda_3 - \lambda_4)L_x$. For a given α_4 we factorize a such that

$$a=a_1e^{a_2},\quad a_1=1+\frac{\alpha_4 a_2}{\tau}. \tag{43}$$

We set $z = (\zeta - a_2)/\tau$ and $\sigma = \alpha_4/\tau a_1$. This leads to the equation

$$\sigma=(1+e^{\zeta})/\zeta,\quad 0\le\sigma<\infty. \tag{44}$$

Equation (44) has infinitely many solutions $\zeta_m(\sigma)$ in the complex plane for a fixed $\sigma > 0$. We want to choose α_4 such that the least real parts of z are as large as possible. The least real part of z corresponds to the least real part of ζ. A special solution of (44) is

$$\zeta^*=1+e^{-\zeta^*},\quad \sigma^*=e^{\zeta^*},$$

which gives $\sigma^* \approx 3.59$. It is shown in [14] that

$$\max_{0<\sigma<\infty}\min_m \text{Re}\,\zeta_m(\sigma)=\zeta^*. \tag{45}$$

Thus the optimum $\alpha_4 = \alpha_4^*$ satisfies

$$\alpha_4^*=\tau a_1\sigma^*. \tag{46}$$

We introduce this into (43), set $\kappa = e^{a_2} = a/a_1$ and get

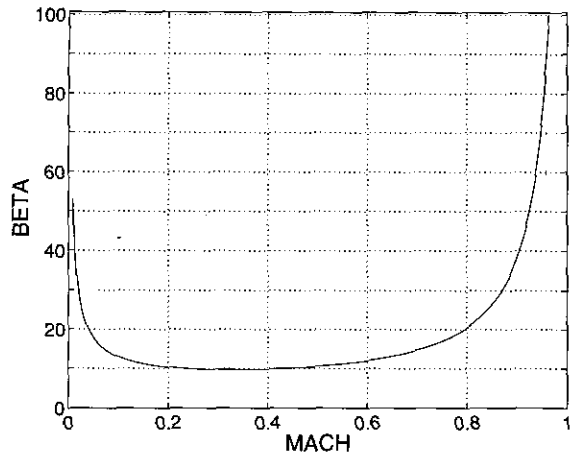

FIG. 1. Scaling due to the Mach number.

$$\frac{1-\sigma^* \log \kappa}{\kappa} = \frac{1}{a}.$$

This shows that κ is a function $\kappa(M)$ of M, and

$$\alpha_4^*(M) = \frac{L_x}{c}\beta_4(M),$$

where $\beta_4(M) = 2\sigma^*\kappa(M)/(1 - M^2)$. Note that we obtain the expected scaling by L_x/c. The function $\beta_4(M)$ is plotted in Fig. 1.

To study the choice of α_3 we set $\alpha_4 = 0$. This leads to $\alpha_3^*(M) = \alpha_4^*(M)$. The steady conditions keep Ψ_1 fixed in time at the inflow boundary. Thus the added non-reflecting term is zero, and hence, the choice of α_1 has no effect on the solution.

5. NUMERICAL EXAMPLES

The Euler equations in conservative form are

$$\frac{\partial W}{\partial t} + \frac{\partial F}{\partial x} + \frac{\partial G}{\partial y} = 0,$$

where

$$W = \begin{pmatrix} \rho \\ \rho u \\ \rho v \\ E \end{pmatrix}, \quad F = \begin{pmatrix} \rho u \\ \rho u^2 + p \\ \rho uv \\ u(E+p) \end{pmatrix}, \quad G = \begin{pmatrix} \rho u \\ \rho uv \\ \rho v^2 + p \\ v(E+p) \end{pmatrix},$$

and

$$p = (\gamma - 1)\left(E - \rho\frac{u^2 + v^2}{2}\right).$$

We use $\gamma = 1.4$.

5.1. *Description of the Experiments*

In the numerical calculations presented here we use a finite-volume technique with artificial dissipation in space and a Runge–Kutta procedure in time [13]. If we disregard the artificial dissipation the operators in space are second-order central differences if the grid is perfectly uniform.

We are interested in the convergence as function of β when the weights on the non-reflecting terms are $\alpha_i = \beta_i(L_x/c)$. We present the results as functions of β, but we omit the factor $\sqrt{\gamma}$ when calculating c. The weights are thus

$$\alpha_i = \beta_i \frac{L_x}{c}\sqrt{\gamma}, \tag{47}$$

where $\sqrt{\gamma} \approx 1.18$. Some experiments with different values of γ suggest that the scaling with L_x/c is more general. Unless otherwise mentioned we set $\beta_1 = \beta_2 = \beta_3 = \beta_4 = \beta$ in all numerical examples.

We consider the boundary conditions

S, the steady conditions in Section 2

C, the combined conditions in Section 3

N, the conditions $\Psi_{in} = f$,

where f is the free-stream value far outside the boundary. The mean values of the converged S-solutions are used for the missing outflow values of f needed for the N-conditions. The mean value parts of the S- and C-conditions are always (20), (21), and (24). No non-reflecting mean value terms are used in the numerical examples. The reasons for that are given in Section 3.

The goal is to obtain the steady S-solution rapidly by using the C-conditions. We are thus interested in the difference to the steady S-solution during the computation. We will refer to this difference as the error, even if the S-solution is not the exact solution of the mathematical problem. In some cases (II.a,III) the S-solutions do not converge without the non-reflecting terms. In these cases the solutions are compared to a converged C-solution, which well satisfies the steady conditions. All results are measured using the norm

$$\|w\| = \left(\frac{1}{n_x n_y}\sum_{i=1}^{n_x}\sum_{j=1}^{n_y} w_{ij}^2\right)^{1/2},$$

where n_x and n_y are the number of grid lines in the x- and y-directions. Only the pressure is considered when solutions are compared. In convergence history plots the norms are scaled such that the logarithm starts from zero.

Unless otherwise mentioned $\rho_{-\infty} = p_{-\infty} = 1$. No outflow data are given. Therefore we use the mass flow condition (24) at the outflow boundary. We must be careful when choosing the initial solution when using this condition; otherwise the

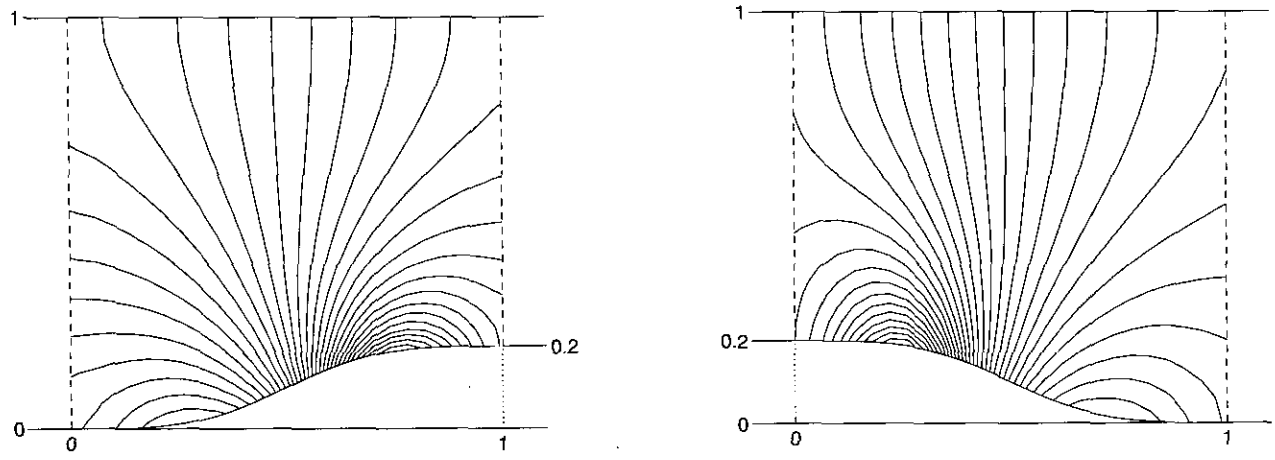

FIG. 2. Flow in channels, Isobars. Channel I, $M_{-\infty} = 0.4$; Channel II, $M_{-\infty} = 0.8$.

solution may not converge. The initial state in the numerical examples is

$$\rho(x, y) = \frac{\rho_{-\infty}}{q(x)}, \quad p(x, y) = \frac{p_{-\infty}}{q(x)},$$

$$u(x, y) = u_{-\infty} q(x)^2, \quad v(x, y) = 0,$$

where $q(x) = (y_2(a) - y_1(a))/(y_2(x) - y_1(x))$ and y_2 and y_1 are the upper and lower channel walls.

5.2. *Experimental Optimization of the Coefficients*

We use the geometries in Fig. 2. The upper and lower boundaries are solid walls. The dashed lines are the artificial inflow and outflow boundaries. Outside these artificial boundaries the channel walls are infinitely long straight lines. We use uniform 25×25 grids. The Mach numbers of the test problems are given in Table I. The six test problems are solved with a common value β for the coefficients β_i in (34). The values 0, $\frac{1}{4}$, $\frac{1}{2}$, 1, 2, 4, 8, 16 are tested. We observe the number of time steps needed to reduce the error to 10^{-5}. The results are plotted in Fig. 3a. Dashed lines correspond to Channel I, and solid lines to Channel II. Results for Mach numbers (a), (b), and (c)-are labeled "○," "×", and "+" respectively. The best results (or very close to the best ones) are obtained for $\beta = 2$ in all six cases.

We also investigate each β_i individually. It turns out that the convergence is independent of β_1. This is due to the fact that Ψ_1 is kept fixed at the inflow boundary by the steady conditions. The corresponding non-reflecting term is thus zero. The results for β_2 suggest that the value of β_2 can be reduced. Figure 3b shows results when $(\beta_1, \beta_2, \beta_3, \beta_4) = (0, \beta/2, \beta, \beta)$. The convergence is now clearly improved for larger values of β.

Scaling with the speed of sound. The results in Fig. 3 are obtained for problems with $c = \sqrt{\lambda p/\rho} \approx 1.18$. If we use the inflow data $\rho_{-\infty} = 1/(p_{-\infty}) = 4$, the speed of sound is reduced by a factor of 4. Figure 4a compares results for problem II.a with the original speed of sound to results with the reduced speed of sound. These results are labelled "×" and "○," respectively. The figure confirms the scaling with the speed of sound in (47).

Scaling with the length of the channel. Consider the geometries in Fig. 5. The grids are 25×50 and 50×25, respectively. The inflow mach number is 0.4. The number of iterations needed to reduce the error to 10^{-5} for different values of β are shown in Fig. 4b. Results for problem II.c are also shown. The results of Channels II, III, IV are labelled "×," "○," "+," respectively. The figure confirms the scaling with the length of the channel in condition (47).

Scaling depending on the Mach number. The optimum β_3, β_4, obtained by the one-dimensional analysis in Section 4.3, are shown in Fig. 1. The numerical experiments above give smaller optimum parameters. On the other hand, it is confirmed that the optimum parameters do not depend much on Mach numbers away from $M = 0$ and $M = 1$. The largest Mach

TABLE I

The Mach Numbers in Channels I and II

	$M_{-\infty}$		M_∞	
	I	II	I	II
a	0.5	0.8	0.73	0.52
b	0.4	0.6	0.54	0.44
c	0.3	0.4	0.39	0.31

Note. Only $M_{-\infty}$ is used as data, while M_∞ are values obtained from the converged numerical solutions.

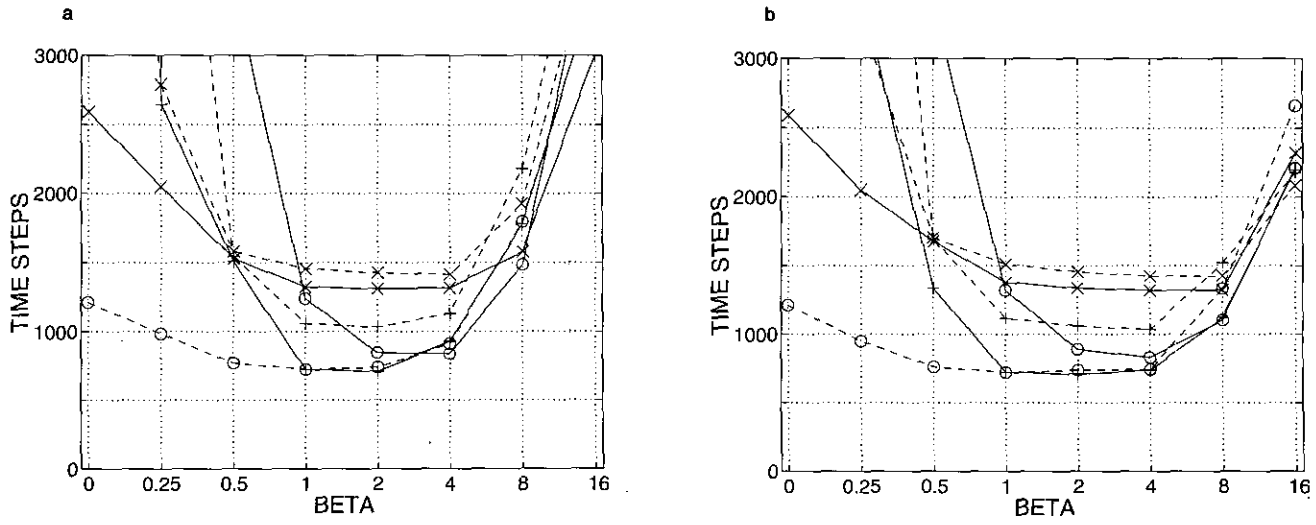

FIG. 3. Convergence for different values of β for six test problems: (a) $\beta_1 = \beta_2 = \beta_3 = \beta_4 = \beta$; (b) $2\beta_2 = \beta_3 = \beta_4 = \beta$.

number in the numerical examples is found in Problem II.a, where $M_{-\infty} = 0.8$, but $M_\infty \approx 0.52$. Experiments with $M \approx 0.85$ in the whole region give as expected a larger optimum α. These experiments are otherwise less interesting. Almost straight channel walls are used in the interior to keep the flow subsonic. It can be pointed out that the steady conditions become ill conditioned when the Mach number is close to one.

5.3. *The Convergence with Large Non-reflecting Terms*

The convergence of the mean values of the solution is studied in Section 3.2. Consider the mean value conditions (20), (21), (25). For a large α equations (26), (27) show that $\hat{\Psi}_4(b, t) \approx \hat{\Psi}_4(b, 0)$ for a long time. During this first phase the initial state $\hat{\Psi}_4(x, t)$ is approximately replaced by $\hat{\Psi}_4(b, 0)$ in the whole domain. In the second phase the solution slowly tends to the correct steady state.

If we consider the whole solution, not just the mean values, a large α still implies that Ψ_{in} for a long time almost stays at the initial state at the boundary. Thus the solution can be expected to initially tend to that steady solution which is obtained with the boundary condition $\Psi_{in}(t) = \Psi_{in}(0)$. The S-values of $\hat{\Psi}_{in}$ are only slowly allowed to enter the region by the non-reflecting boundary terms. The slowly entering values become noticeable when the residual has been decreased enough by the rapid initial convergence. We thus expect a similar two-phase behavior as for the mean values. This behavior is confirmed by Fig. 6b. It is not due to the mean values, since no non-reflecting mean value term is used. We do not want the two-phase behavior in practical applications. The boundary conditions should be

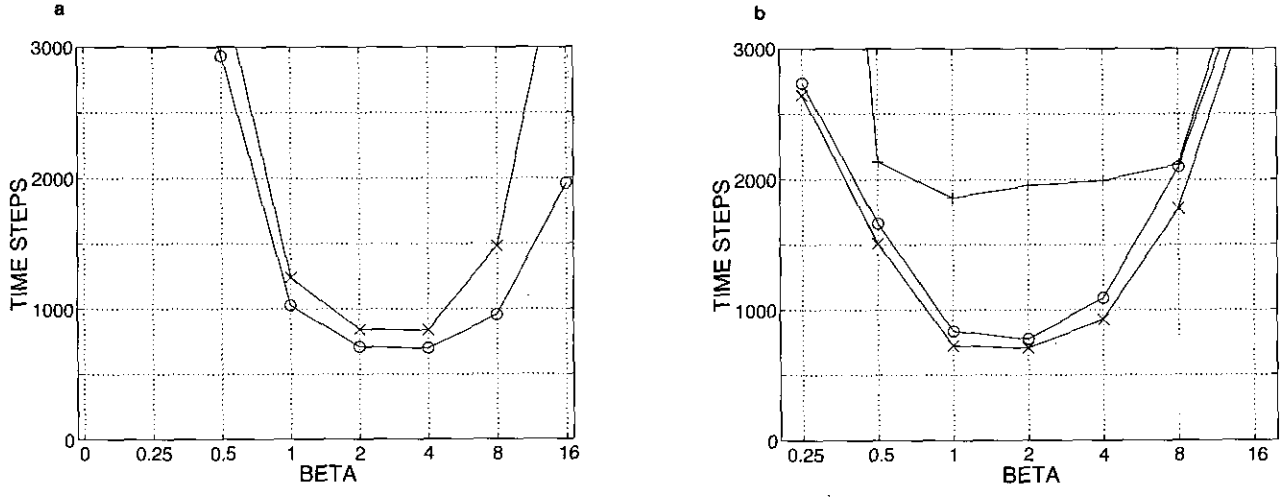

FIG. 4. Verifying the scaling with the speed of sound (a) and the length of the channel (b).

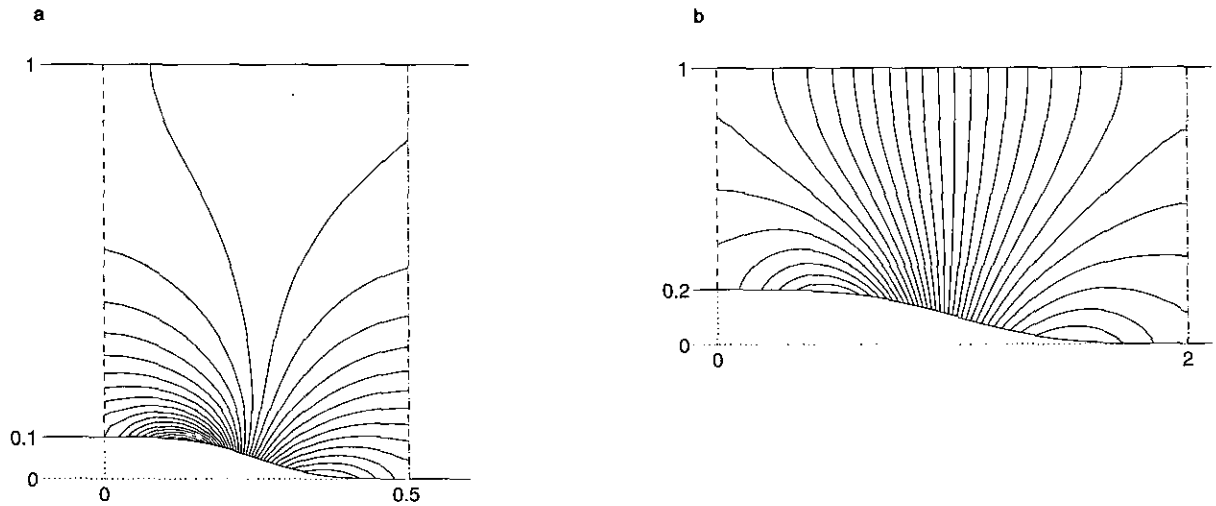

FIG. 5. Isobars in short and long channels: (a) Channel III; (b) Channel IV.

balanced such that the solution converges rapidly to the correct steady state all the time.

Figure 6a shows the number of time steps needed to reduce the error and residual to three levels. The levels for the residual are 10^{-4} (○), 10^{-5} (×), and 10^{-6} (+). The levels for the error are 10 times larger. These results are obtained for problem I.a. Note that the slower convergence for larger β is hard to detect on the residual. We can check that a solution satisfies the unmodified steady conditions before accepting it.

5.4. *An Example with Correctly Balanced Boundary Conditions*

We solve problem II.a using the C-conditions with $\beta_i = 2$ and for comparison, also with the N- and S-conditions. The convergence histories of the error and residual are plotted in Fig. 7. Note that the convergence of the C- and R-residuals are very similar, and that the C-error converges at about the same rate. This indicates that the C-conditions are implemented in an optimum way. Note that these C- and S-results are obtained without using any outflow data at all.

6. CONCLUSIONS

We study how the steady and non-reflecting parts of the combined conditions should be balanced to optimize the convergence to an accurate steady state. The best results, or very close to the best ones, are obtained if the weights on the non-reflecting terms are $\alpha_i \approx 2L/c$. Here L is the length of the channel and

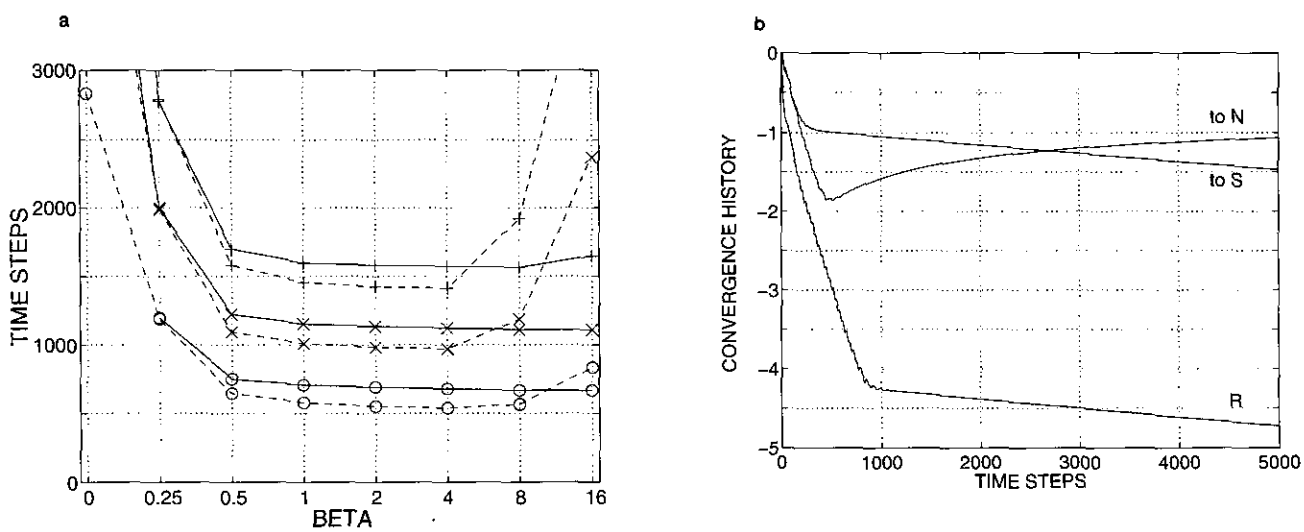

FIG. 6. Behavior for large values of β: (a) Slow convergence (—) for $\beta \geq 8$ is less obvious on the residual (–). (b) Slow convergence to S, but rapid initial convergence to the wrong state N.

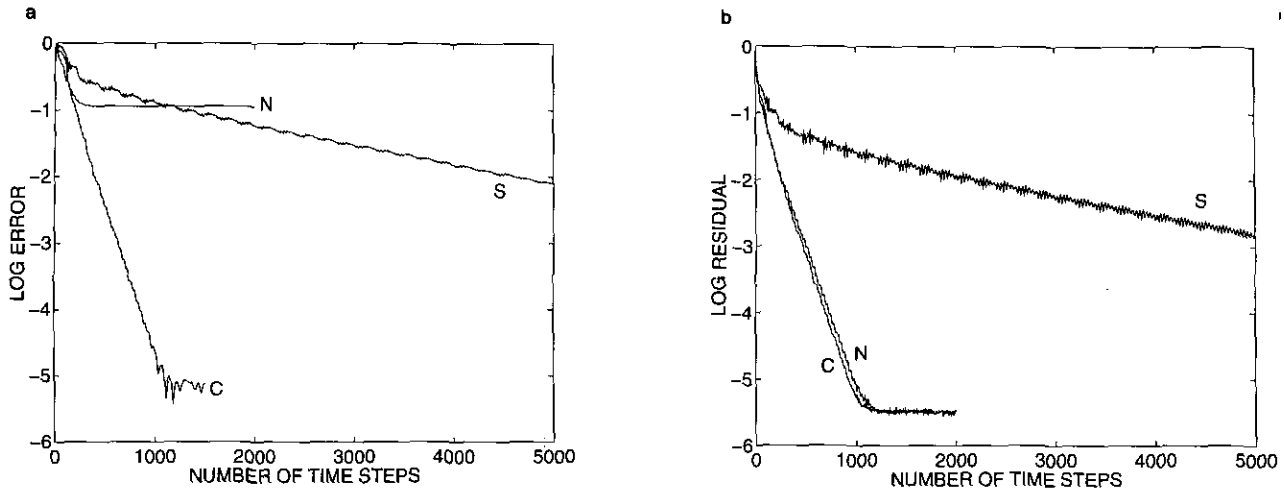

FIG. 7. The convergence when the boundary conditions are correctly balanced: (a) The error. (b) The residual.

c is the speed of sound. This optimum is valid for Mach numbers away from $M = 0$ and $M = 1$. There is usually a relatively wide interval where the optimum parameters can be chosen. Too large weights on the non-reflecting terms lead to slower convergence. This may be hard to detect on the residual. Some experiments indicate that we get a more robust method if α_2 is reduced to $\alpha_2 = L/c$. In numerical examples with correctly balanced boundary conditions we obtain the accuracy of the steady conditions and the convergence rate of the characteristic ones. These are the best results that can be expected.

The mean values can be treated in different ways by the boundary conditions. If the steady mean value conditions are chosen correctly, the convergence of the mean value are very rapid. Non-reflecting mean value conditions do in this case not accelerate the convergence.

ACKNOWLEDGMENTS

This work has been supported financially by the Swedish Research Counsil for Engineering Sciences (TFR).

REFERENCES

1. A. Bayliss and E. Turkel, *J. Comput. Phys.* **48,** 182 (1982).
2. B. Engquist and L. Halpern, *Appl. Numer. Math.* **4,** 21 (1988).
3. B. Engquist and A. Majda, *Math. Comput.* **31,** 629 (1977).
4. B. Engquist and A. Majda, *Commun. Pure Appl. Math.* **32,** 312 (1979).
5. L. Ferm, *J. Comput. Phys.* **78,** 94 (1988).
6. L. Ferm, *J. Comput. Phys.* **91,** 55 (1990).
7. L. Ferm and B. Gustafsson *Comput. Fluids* **10,** 261 (1982).
8. M. Giles, *AIAA J.* **28,** 2050 (1990).
9. D. Givoli, *J. Comput. Phys.* **94,** 1 (1991).
10. G. W. Hedstrom, *J. Comput. Phys.* **30,** 333 (1979).
11. R. L. Higdon, *SIAM J. Numer. Anal.* **31,** 64 (1994).
12. J. B. Keller and D. Givoli, *J. Comput. Phys.* **82,** 172 (1989).
13. A. Rizzi and L. E. Eriksson, *J. Fluid. Mech.* **148,** 45 (1984).
14. D. Rudy and J. C. Strikwerda, *J. Comput. Phys.* **36,** 55 (1980).
15. D. Rudy and J. C. Strikwerda, *J. Comput. Fluids* **9,** 327 (1981).